Nuclear Engineering and Design 256 (2013) 75–86

Contents lists available at SciVerse ScienceDirect

Nuclear Engineering and Design

journal homepage: www.elsevier.com/locate/nucengdes

Physics-based modelling of fission gas swelling and release in UO_2 applied to integral fuel rod analysis

Giovanni Pastore [a], Lelio Luzzi [a,*], Valentino Di Marcello [b], Paul Van Uffelen [b]

[a] Politecnico di Milano – Department of Energy, Enrico Fermi Center for Nuclear Studies (CeSNEF), via Ponzio 34/3, I-20133 Milano, Italy
[b] European Commission – Joint Research Centre, Institute for Transuranium Elements (ITU), Hermann-von-Helmholtz-Platz 1, D-76344 Karlsruhe, Germany

HIGHLIGHTS

- Physics-based model for the coupled fission gas swelling and release in UO_2.
- Improvement of the White model for grain-face gas bubble coalescence.
- Evaluation of the dependence of the phenomena on the local hydrostatic stress.
- Implementation in the TRANSURANUS code for integral fuel rod analysis.
- Satisfactory agreement between model predictions and experimental data.

ARTICLE INFO

Article history:
Received 18 May 2012
Accepted 4 December 2012

ABSTRACT

A physics-based model is developed for analysing the coupled phenomena of fission gas swelling and release in UO_2 fuel during irradiation. The model is featured by a level of complexity suitable for application to integral fuel rod analysis and consistent with the uncertainties pertaining to some parameters. The emphasis is on the modelling of the grain-face gas bubble development and the related dependence of the fission gas swelling and release on the local hydrostatic stress, which is of special importance for the analysis of the fuel behaviour during power ramps and pellet-cladding mechanical interaction conditions. The applicability of the new model to integral fuel rod analysis is verified through implementation and testing in the TRANSURANUS fuel rod analysis code. In the frame of the IAEA co-ordinated research project on Fuel Modelling at Extended Burn-up FUMEX-III, the model is applied to the simulation of irradiation experiments from the OECD/NEA International Fuel Performance Experiments database. The comparison of the results with the available experimental data of fission gas swelling and release at moderate burn-up is presented as a first step of validation, pointing out an encouraging predictive accuracy for different irradiation conditions, without any fitting applied to the model parameters.

1. Introduction

Modelling of the processes induced by the generation of the fission gases xenon and krypton in uranium dioxide fuel is essential for analysing the thermal–mechanical behaviour of the nuclear fuel rods employed in current light water reactors (LWR). On the one hand, the fission gases tend to precipitate into bubbles resulting in fuel swelling, which promotes pellet-cladding gap closure and the ensuing pellet-cladding mechanical interaction (PCMI). On the other hand, fission gas release (FGR) to the fuel rod free volume causes pressure build-up and thermal conductivity degradation of the rod filling gas. The kinetics of both fission gas swelling and thermal release is determined by the development of the grain-face gas bubbles (White, 2004). Lenticular bubbles grow on the grain faces during irradiation via inflow of gas from within the grains and vacancy absorption, thereby contributing to gas retention and swelling. The growing bubbles eventually inter-connect, leading to the formation of continuous pathways to the fuel exterior and FGR. The inherently coupled kinetics of the fission gas swelling and release calls for the development of physics-based models of these phenomena to be employed in the fuel rod analysis codes (Aybar and Ortego, 2005; Calvin and Nowak, 2010; Geelhood, 2011;

Abbreviations: AGR, Advanced Gas-cooled Reactor; BWR, boiling water reactor; EOL, end of life; FGR, fission gas release; FUMEX, Fuel Modelling at Extended Burn-up; IAEA, International Atomic Energy Agency; IFPE, International Fuel Performance Experiments; LWR, light water reactor; NEA, Nuclear Energy Agency; PCMI, pellet-cladding mechanical interaction; PWR, pressurized water reactor; OECD, Organisation for Economic Co-operation and Development; RTL, ramp terminal level; SEM, scanning electron microscopy.

* Corresponding author. Tel.: +39 02 2399 6326; fax: +39 02 2399 6309.
E-mail address: lelio.luzzi@polimi.it (L. Luzzi).

0029-5493/$ – see front matter © 2012 Elsevier B.V. All rights reserved.
http://dx.doi.org/10.1016/j.nucengdes.2012.12.002

Nomenclature

A_{gf}	projected area of grain-face bubbles (m^2)
b	resolution parameter (s^{-1})
B	model parameter (m)
C_b	concentration of intra-granular gas in bubbles (m^{-3})
C_s	concentration of intra-granular gas as single atoms (m^{-3})
C_t	concentration of intra-granular gas (as single atoms + in bubbles) (m^{-3})
D_{eff}	effective diffusion coefficient ($m^2\ s^{-1}$)
D_s	single gas atom diffusion coefficient ($m^2\ s^{-1}$)
D_v	vacancy diffusion coefficient in grain boundaries ($m^2\ s^{-1}$)
F	fission rate density ($m^{-3}\ s^{-1}$)
F_c	fraction of grain faces covered by bubbles (fractional coverage)
$F_{c,sat}$	fractional coverage at grain face saturation
g	trapping parameter (s^{-1})
k	Boltzmann constant ($J\ K^{-1}$)
l_f	length of a fission fragment track (m)
m	number of fission gas atoms per intra-granular bubble
n_{fgr}	number of fission gas atoms released to the fuel rod free volume
n_g	number of fission gas atoms per grain-face bubble
N_{gf}	number density of grain-face bubbles per unit surface (m^{-2})
$N_{gf,0}$	initial number density of grain-face bubbles per unit surface (m^{-2})
N_{ig}	number density of intra-granular bubbles per unit volume (m^{-3})
n_v	number of vacancies per grain-face bubble
p	gas pressure in grain-face bubbles (Pa)
p_{eq}	mechanical equilibrium pressure of the gas in grain-face bubbles (Pa)
q_s	specific power ($W\ kg^{-1}$)
r	radial co-ordinate in the spherical grain (m)
R_{gf}	radius of curvature of grain-face bubbles (m)
r_{gr}	grain radius (m)
R_{ig}	radius of intra-granular bubbles (m)
S	model parameter
t	time (s)
T	temperature (K)
V	volume of fuel (m^3)
V_{gf}	volume of grain-face bubbles (m^3)
Z_0	radius of influence of a fission fragment track (m)
β	fission gas generation rate ($m^{-3}\ s^{-1}$)
γ	UO_2/gas specific surface energy ($J\ m^{-2}$)
δ_g	thickness of the diffusion layer in grain boundaries (m)
$(\Delta V/V)_{ig}$	volumetric intra-granular fission gas swelling
$(\Delta V/V)_{gf}$	volumetric grain-face fission gas swelling
θ	semi-dihedral angle of the grain-face bubbles (°)
σ_h	hydrostatic stress (one-third of the trace of the stress tensor) (Pa)
τ_1	conditioning time (s)
τ_{2a}	power increasing time during the ramp (s)
$\varphi(\theta)$	geometric factor relating the volume of a lenticular bubble to that of a sphere
ω	Van der Waals' volume of a fission gas atom (m^3)
Ω_{gf}	atomic (vacancy) volume in grain-boundary bubbles (m^3)
Ω_{ig}	volume per gas atom in intra-granular bubbles (m^3)

Lee et al., 2011; Rossiter, 2011). As of today, however, empirical or semi-empirical approaches are often adopted (e.g., Griger and Gadó, 2007; Harriague et al., 1980; Lassmann et al., 2011; Mikityuk and Shestopalov, 2011). These models are efficient to use but unfit for providing insight into the underlying mechanisms, and cannot be applied beyond their range of calibration.

A topical modelling issue concerns the role of the compressive hydrostatic stress in the fuel, acting to constrain the growth of the grain-face gas bubbles and consequently affecting both the fission gas swelling and release. This effect is of particular significance under the conditions of strong PCMI (e.g., resulting from a power ramp), when high compressive hydrostatic stress may develop in the fuel due to cladding restraint (Van Uffelen et al., 2004). Zimmermann (1978) revealed that mechanical restraint reduced the fission gas swelling by a factor of 2 in comparison with unrestrained swelling in isothermal irradiation tests. Kogai et al. (1988) and Mogensen et al. (1993) emphasized the dependence of the FGR behaviour on the extent of PCMI during power bump tests. Kashibe and Une (1997) observed considerable suppression of the fission gas swelling by external restraint in unirradiated UO_2 fuel during annealing at temperatures up to 1800 °C. Nakamura et al. (1999) concluded that a sudden increase of the FGR during a reduction of the linear heat rate from 40 to 20 $kW\ m^{-1}$ ensued from the reduction of the hydrostatic stress in the fuel, reflecting a thermal stress variation. Physics-based models of fission gas swelling and release currently implemented in the fuel rod analysis codes generally disregard or approximate the hydrostatic stress by a uniform value based on the rod internal pressure and/or the pellet-cladding contact pressure (e.g., Bernard and Bonnaud, 1997; Khvostov et al., 2011; Koo et al., 2000; Lassmann et al., 2011; Suzuki and Saitou, 2006; Van Uffelen et al., 2004). In view of the current tendency to extend the discharge burn-up and the flexibility of use (load-following) of the nuclear fuel, the improved modelling of the fission gas swelling and release under PCMI conditions is highly advisable (OECD/NEA, 2004). For this purpose, it is essential to develop models that properly take into account the dependence of the fission gas swelling and release kinetics on the local hydrostatic stress, and that are applicable to the integral thermal–mechanical analysis of the fuel rods.

In this paper, a physics-based model of fission gas swelling and release in UO_2 fuel during irradiation is developed and tested in the TRANSURANUS fuel rod analysis code (Lassmann, 1992). The modelling approach is based on a pragmatic compromise between a physics-based treatment and the efficiency of computation needed for application to integral fuel rod analysis and the related engineering purposes. The emphasis is on the development of the grain-face gas bubbles, which underlies the coupling between the fission gas swelling and release, and the dependence of these phenomena on the local hydrostatic stress in the fuel. The physical description is based on models presented earlier (Speight, 1969; Speight and Beere, 1975; Veshchunov, 2008; White, 2004; White and Tucker, 1983) for the fundamental mechanisms, some of which are improved in this work. These models are combined in a simple and practical treatment, aimed to grasp the main peculiarities of the fission gas swelling and release. The work was carried out in the frame of the co-ordinated research project on Fuel Modelling at Extended Burn-up FUMEX-III of the IAEA (Killeen et al., 2009; Schubert et al., 2011).

The paper is organized as follows. In Section 2, the main features of the new model are outlined. In Section 3, the model is applied as stand-alone version and evaluated by comparison of the predictions with experimental data of grain-face fission gas swelling. In Section 4, integral fuel rod analyses carried out using the TRANSURANUS code and adopting the new model are presented, and the results are compared with experimental data of FGR. Conclusions are drawn is Section 5.

2. Model description

The fundamental physical processes, which control the kinetics of fission gas swelling and release in irradiated UO_2 fuel, may be summarised as follows (Garcia et al., 2012; Olander, 1976; Van Uffelen et al., 2010; White, 2004; White and Tucker, 1983). Fission gas atoms generated in the fuel grains diffuse towards the grain boundaries through repeated trapping in and irradiation-induced resolution from nanometre-size intra-granular gas bubbles. The contribution of intra-granular bubbles to fission gas swelling (intra-granular swelling) is generally less important than the swelling due to grain-face bubbles, at least for burn-up below about 45 GWd/t (Kashibe et al., 1993). Although a part of the gas atoms that reach the grain boundaries is dissolved back to the grain interior by irradiation, the majority of the gas diffuses into grain-face gas bubbles acting to increase the bubble internal pressure and generally maintaining bubbles in a non-equilibrium state. Micron-size grain-face bubbles grow with inflow of gas atoms and with absorption of vacancies driven by the bubble over-pressure, giving rise to grain-face swelling. Bubble growth brings about bubble coalescence and inter-connection, eventually leading to the formation of a tunnel network through which a fraction of the gas is released to the fuel rod free volume.

The model presented in this paper incorporates the above processes in order to evaluate the kinetics of fission gas swelling and release. The model is kept as simple as possible in view of (i) the efficient application to integral fuel rod analysis and the related stringent computational cost requirements, (ii) the uncertainties pertaining to fuel rod analysis (Lassmann, 1980), and (iii) the uncertainties associated to some of the model parameters like the gas atom diffusion coefficient (Govers et al., 2008; Matzke, 1980; White, 1994; White and Tucker, 1983).

2.1. Intra-granular gas behaviour

The rate equation describing the intra-granular diffusion of fission gas reads in one-dimensional spherical geometry

$$\frac{\partial C_t}{\partial t} = D_{eff}\frac{1}{r^2}\frac{\partial}{\partial r}\left(r^2\frac{\partial C_t}{\partial r}\right) + \beta, \tag{1}$$

where C_t is the intra-granular gas concentration (as single atoms + in bubbles), t the time, D_{eff} the effective gas diffusion coefficient, r the radial co-ordinate in the spherical grain, and β the gas generation rate. The effective diffusion coefficient allows for the effect of repeated trapping in and irradiation-induced resolution from intra-granular bubbles (considered as immobile) and is calculated as (Speight, 1969)

$$D_{eff} = \frac{b}{b+g}D_s, \tag{2}$$

where g is the rate of gas atom trapping into bubbles (trapping parameter), b the rate of irradiation-induced gas atom resolution from bubbles back into the lattice (resolution parameter), and D_s the single gas atom diffusion coefficient in the UO_2 lattice. Eq. (2) entails the assumption that bubbles are effectively saturated giving

$$\frac{C_s}{C_b} = \frac{b}{g}, \tag{3}$$

where C_s is the concentration of gas existing as single atoms, and C_b the concentration of gas in bubbles. In this respect, the ratio $b/(b+g)$ may be considered as the fraction of intra-granular gas that exists as single atoms and is therefore available for diffusion. The trapping and resolution parameters are calculated as (Ham, 1958; White and Tucker, 1983)

$$g = 4\pi D_s R_{ig} N_{ig}, \tag{4}$$

$$b = 3.03F\pi l_f (R_{ig} + Z_0)^2, \tag{5}$$

where R_{ig} is the mean radius of intra-granular bubbles, N_{ig} the number density of intra-granular bubbles, F the fission rate density, l_f the length of a fission fragment track, and Z_0 the radius of influence of a fission fragment track. It is assumed that the intra-granular bubbles are spherical, homogeneously distributed and of equal size (Ham, 1958; Lösönen, 2002; Olander, 1976; Turnbull, 1971; White and Tucker, 1983). A fixed number density of intra-granular bubbles, N_{ig}, is further considered in line with Speight (1969) and the observation that the bubble number density rapidly stabilizes during irradiation (Turnbull, 1971; White and Tucker, 1983). For bubble radii ranging from 0.5 to 2 nm, the radius of a bubble containing m fission gas atoms may be calculated as (Olander and Wongsawaeng, 2006)

$$R_{ig} = Bm^{1/3}, \tag{6}$$

where $B = (3\,\Omega_{ig}/4\pi)^{1/3} = 2\times10^{-10}$ m, and Ω_{ig} is the volume per gas atom contained in the bubble. The number of fission gas atoms contained in each bubble, m, is

$$m = \frac{C_b}{N_{ig}}, \tag{7}$$

where, considering that $C_t = C_s + C_b$ and under the condition expressed by Eq. (3), C_b is given by

$$C_b = \frac{g}{g+b}C_t. \tag{8}$$

The above treatment of the intra-granular gas behaviour is intended as a simplified approach, aimed at estimating in a preliminary way the effect of intra-granular bubbles on fission gas diffusion and the intra-granular swelling. The fractional volume intra-granular swelling, normalized to the unit volume of fuel, V, is given as

$$\left(\frac{\Delta V}{V}\right)_{ig} = N_{ig}\left(\frac{4}{3}\pi R_{ig}^3\right). \tag{9}$$

2.2. Grain-face gas behaviour

In order to obtain a suitable description of the grain-face bubble development in terms of complexity, the following main assumptions are made:

- Peculiarities related to the presence of grain edges (where three grains meet) are neglected (e.g., Kogai, 1997; Massih and Forsberg, 2008).
- An initial number density of grain-face bubbles (nucleation centres) is considered, and further nucleation during the irradiation is neglected (one-off nucleation, e.g., White, 2004).
- The absorption rate of gas at the grain-face bubbles is assumed to equal the arrival rate of gas at the grain boundaries. The validity of this approximation follows from the large difference between the lattice and grain-boundary diffusivities of gas atoms (Olander and Van Uffelen, 2001; White, 2004).
- All the grain-face bubbles have, at any instant, equal size and equal lenticular shape of circular projection. A uniform, average bubble size is therefore considered at any instant (e.g., Veshchunov, 2008).
- The flux of gas atoms dissolved from the grain faces back to the grain interior by irradiation is neglected (Rest, 2003).

The fractional volume grain-face swelling, normalized to the unit volume of fuel, is then given as

$$\left(\frac{\Delta V}{V}\right)_{gf} = \frac{1}{2}\frac{N_{gf}}{(1/3)r_{gr}}\left(\frac{4}{3}\pi\varphi(\theta)R_{gf}^3\right), \tag{10}$$

where N_{gf} is the number density of grain-face bubbles per unit surface, r_{gr} the grain radius, θ the bubble semi-dihedral angle, $\varphi(\theta)$ the geometric factor relating the volume of a lenticular-shape bubble to that of a sphere, which is $1-1.5\cos\theta+0.5\cos^2\theta$, and R_{gf} the bubble radius of curvature. The factor 1/2 is introduced in Eq. (10) because a grain-face bubble is shared by two neighbouring grains. A physics-based calculation of the bubble size and number density is included in the present model, in order to allow for their time dependence and interrelation. For this purpose, the development of grain-face bubbles may be conveniently considered as resulting from the following processes:

- The growth of bubbles through the collection of fission gas atoms and vacancies.
- The mutual interaction between bubbles through coalescence leading to larger but fewer bubbles.
- The release of fission gas from the grain faces to the fuel rod free volume.

The modelling of these processes is discussed in Sections 2.2.1, 2.2.2 and 2.2.3.

2.2.1. Bubble growth

In general, grain-face gas bubbles exist in a non-equilibrium state and tend to restore equilibrium by absorption or emission of vacancies. The mechanical equilibrium pressure of the gas, p_{eq}, in a lenticular bubble of circular projection is given by

$$p_{eq}=\frac{2\gamma}{R_{gf}}-\sigma_h, \tag{11}$$

where γ is the UO_2/gas specific surface energy and σ_h is the hydrostatic stress (considered to be negative if the solid medium is under compression). The Speight and Beere (1975) model describes the growth (or shrinkage) of the grain-face bubbles as proceeding by absorption (or emission) of vacancies generated on the grain boundaries. The vacancy absorption/emission rate at a bubble is given by

$$\frac{dn_v}{dt}=\frac{2\pi D_v\delta_g}{kTS}(p-p_{eq}), \tag{12}$$

where n_v is the number of vacancies in the bubble, D_v the vacancy diffusion coefficient in grain boundaries, δ_g the thickness of the diffusion layer in grain boundaries, k the Boltzmann constant, T the temperature, and S is calculated as

$$S=\frac{-((3-F_c)\cdot(1-F_c)+2\ln(F_c))}{4}, \tag{13}$$

with F_c being the fraction of grain faces covered by bubbles (fractional coverage). For a Van der Waals' gas, the pressure of the gas in the bubble, p, may be written as

$$p=\frac{kT}{\Omega_{gf}}\frac{n_g}{n_v}, \tag{14}$$

where Ω_{gf} is the atomic (vacancy) volume in grain-face bubbles and n_g the number of gas atoms per bubble. The volume, V_{gf}, of a bubble comprising n_g fission gas atoms and n_v vacancies is then given by

$$V_{gf}=n_g\omega+n_v\Omega_{gf}, \tag{15}$$

where ω is the Van der Waals' volume of a fission gas atom. The above approach was proposed earlier by White (2004) and allows calculating the bubble growth rate based on the rate of inflow of gas atoms along with the rate of absorption (emission) of vacancies at the bubble. Given the volume, V_{gf}, of a lenticular bubble of circular projection, the bubble radius of curvature is

$$R_{gf}=\left(\frac{3V_{gf}}{4\pi\varphi(\theta)}\right)^{1/3}. \tag{16}$$

2.2.2. Bubble coalescence

In the coalescence process, grain-face bubbles intersect and merge into larger but fewer bubbles. Bubble growth brings about mechanical interference between bubbles and coalescence, and consequent progressive reduction in the bubble number density and increase in the average bubble size. In line with White (2004), the coalescence rate may be considered as related to the rate of increase of the bubble projected area on the grain-face, A_{gf}, resulting from bubble growth. In this respect, an increase in the bubble area by an amount dA_{gf} leads to interaction of the bubble with $4N_{gf}dA_{gf}$ surrounding bubbles. It can be demonstrated that this is correct for circular bubbles of the same size in a regular square lattice. Considering each bubble in turn, the total rate of loss of bubbles by coalescence following an increase in the bubble projected area due to bubble growth is given by (White, 2004)

$$\frac{dN_{gf}}{dt}=-2N_{gf}^2\left(\frac{dA_{gf}}{dt}\right)_g, \tag{17}$$

where the factor of 4 is reduced to 2 to avoid counting each interaction twice, and $(dA_{gb}/dt)_g$ denotes the variation of the bubble area owing to bubble growth.

White (2004) assumed that the newly coalesced bubble retains the same area of the two parent bubbles, and did not consider that the bubble number density may decrease directly through gas release when grain face saturation is attained (Section 2.2.3). Veshchunov (2008) modified the model of White by introducing the variation of the average bubble area associated with the coalescence mechanism, and considered the dependence of the bubble number density on the gas release. However, he assumed the bubbles to remain in mechanical equilibrium at any instant and disregarded the effect of the hydrostatic stress. Moreover, he applied the perfect gas law instead of the Van der Waals' equation of state.

In the present work, an improved model is proposed. It is considered that the newly coalesced bubble retains the gas atom and vacancy content of the two parent bubbles, entailing that the coalescence event preserves the volume of the interacting bubbles. This argument leads to the conservation of the total bubble volume per unit surface through coalescence. Moreover, the bubbles can be out of equilibrium and obey the Van der Waals' equation of state (Section 2.2.1). Given that the bubble number density, N_{gf}, decreases through coalescence, the conservation of the total bubble volume per unit surface, $N_{gf}V_{gf}$, implies a variation of the average bubble volume, V_{gf}, due to coalescence. As a result, the rate of variation of the average bubble volume may be expressed as

$$\frac{dV_{gf}}{dt}=\left(\frac{dV_{gf}}{dt}\right)_g+\left(\frac{dV_{gf}}{dt}\right)_c, \tag{18}$$

where $(dV_{gf}/dt)_g$ denotes the variation of the bubble volume owing solely to bubble growth, and $(dV_{gf}/dt)_c$ the variation of the average bubble volume owing solely to coalescence. The variation of the total bubble volume per unit surface is due solely to bubble growth and may be expressed as

$$\frac{d(N_{gf}V_{gf})}{dt}=N_{gf}\left(\frac{dV_{gf}}{dt}\right)_g, \tag{19}$$

where

$$\frac{d(N_{gf}V_{gf})}{dt} = N_{gf}\frac{dV_{gf}}{dt} + V_{gf}\frac{dN_{gf}}{dt}. \quad (20)$$

Superposition of Eqs. (18), (19) and (20) yields

$$\left(\frac{dV_{gf}}{dt}\right)_c = -\frac{V_{gf}}{N_{gf}}\frac{dN_{gf}}{dt}. \quad (21)$$

Given that $V_{gf} \sim A_{gf}^{3/2}$, Eq. (18) implies

$$\frac{dA_{gf}}{dt} = \left(\frac{dA_{gf}}{dt}\right)_g + \left(\frac{dA_{gf}}{dt}\right)_c, \quad (22)$$

where $(dA_{gf}/dt)_c$ denotes the variation of the average bubble area owing solely to coalescence, and Eq. (21) can be written in terms of average bubble area as

$$\left(\frac{dA_{gf}}{dt}\right)_c = -\frac{2}{3}\frac{A_{gf}}{N_{gf}}\frac{dN_{gf}}{dt}. \quad (23)$$

Combining Eqs. (17), (22) and (23), one obtains the rate of loss of bubbles by coalescence according to the new model

$$\frac{dN_{gf}}{dt} = -\frac{6N_{gf}^2}{3+4N_{gf}A_{gf}}\frac{dA_{gf}}{dt}. \quad (24)$$

2.2.3. Fission gas release

The release of fission gas to the fuel rod free volume following inter-connection of grain-face bubbles (thermal release) is modelled based on a principle of grain face saturation (e.g., Bernard et al., 2002): after the fractional coverage attains a saturation value, $F_{c,sat}$ (saturation coverage), the bubble number density and projected area obey the saturation coverage condition (Veshchunov, 2008)

$$F_c = N_{gf}A_{gf} = F_{c,sat}. \quad (25)$$

This implies that a fraction of the gas is released from the grain faces to compensate for bubble growth. More precisely, it is considered that any further bubble growth is balanced by loss of bubbles through gas release in order to maintain the saturation coverage condition, that is, $dF_c/dt = 0$. It follows that the rate of loss of bubbles by gas release after grain face saturation is

$$\frac{dN_{gf}}{dt} = -\frac{N_{gf}}{A_{gf}}\frac{dA_{gf}}{dt}. \quad (26)$$

In general, according to the new model, the rate of variation of the bubble number density is governed by coalescence for $F_c < F_{c,sat}$, and by gas release after attainment of the saturation coverage, and is described by

$$\begin{aligned} \frac{dN_{gf}}{dt} &= -\frac{6N_{gf}^2}{3+4N_{gf}A_{gf}}\frac{dA_{gf}}{dt} && \text{if } N_{gf}A_{gf} < F_{c,sat} \\ \frac{dN_{gf}}{dt} &= -\frac{N_{gf}}{A_{gf}}\frac{dA_{gf}}{dt} && \text{if } N_{gf}A_{gf} = F_{c,sat} \end{aligned}. \quad (27)$$

Eq. (27) allows evaluating the observed reduction in the number density of grain-face bubbles in UO_2 throughout irradiation (White, 2004; White et al., 2006). In Fig. 1, Eq. (27) is compared with the experimental data of bubble number density and corresponding average bubble projected area from (White et al., 2006) (see Section 3). The bifurcation between the dashed line (Eq. (24)) and the full line (Eq. (27)) corresponds to the attainment of the saturation coverage. Eq. (27) appears to reasonably conform to the data.

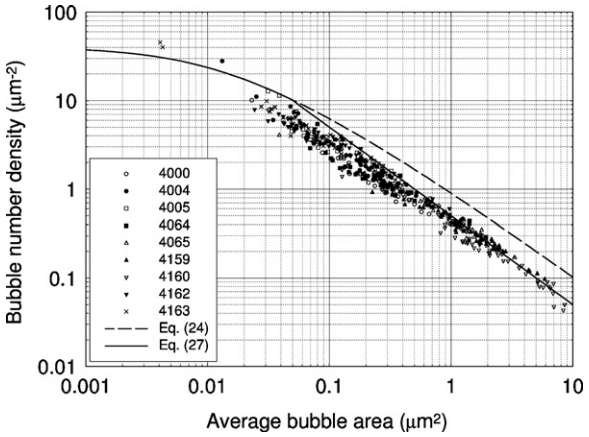

Fig. 1. Variation of the bubble number density with the bubble projected area. Eq. (27) is compared with the experimental data from (White et al., 2006). Eq. (24) is also shown. An initial bubble number density, $N_{gf,0} = 4 \times 10^{13}$ m^{-2}, is considered.

According to the above discussed approach, and considering that each bubble contains n_g fission gas atoms, the FGR is calculated as

$$\begin{aligned} \frac{dn_{fgr}}{dt} &= 0 && \text{if } N_{gf}A_{gf} < F_{c,sat} \\ \frac{dn_{fgr}}{dt} &= n_g\frac{N_{gf}}{A_{gf}}\frac{dA_{gf}}{dt} && \text{if } N_{gf}A_{gf} = F_{c,sat} \end{aligned}, \quad (28)$$

where n_{fgr} is the number of gas atoms released to the fuel rod free volume. This simple representation allows reproducing the incubation behaviour and the dependence of the FGR kinetics on the hydrostatic stress in the fuel, and the coupling with the swelling.

The values adopted for the model parameters are summarised in Table 1.

3. Model testing as stand-alone version

The new model of fission gas swelling and release was firstly coded as stand-alone version, namely, a computer program was developed that receives the fuel fabrication data, specific power, temperature and hydrostatic stress as input and allows performing 'point' fuel analyses. The program incorporates the features described in Section 2 and was employed for the simulation of irradiation experiments from the International Fuel Performance Experiments (IFPE) database (Sartori et al., 2010), as discussed in Sections 3.1 and 3.2.

3.1. Experimental database

The experiments of the AGR/Halden Ramp Test Programme (White et al., 2006) involved the power ramp test of Advanced Gas cooled Reactor (AGR) UO_2 fuel rods in the Halden Reactor, after base-irradiation up to burn-up of around 21 GWd/t. Scanning electron microscopy (SEM) examinations of the irradiated fuel were performed to study the fission gas swelling due to grain-face gas bubbles. The results of the study were made available through the IFPE database. The main information regarding the different irradiation tests and SEM examinations, on which the experimental data of grain-face swelling considered in the present work are referred to, is given in Table 2. The fuel rods were subjected to either power ramps or power cycling. The schematic of the ramp tests is presented in Fig. 2 and the times and powers of each stage are summarised in Table 3. The ramps denoted as slow are those in which the power increasing time, τ_{2a}, is of the order of 45 min and the fast ramps are those for which τ_{2a} lies within the range 1–2 min.

Table 1
Values adopted for the model parameters.

Symbol	Value/expression	Reference(s)
D_s	$D_1 + D_2 + D_3$ ($m^2\ s^{-1}$) $D_1 = 7.6 \times 10^{-10} \exp(-4.86 \times 10^{-19}/kT)$ $D_2 = 3.22 \times 10^{-16} \times (q_s \times 10^{-3})^{1/2} \exp(-1.90 \times 10^{-19}/kT)$ D_3 not considered T: temperature (K) q_s: specific power ($W\ kg^{-1}$)	Turnbull et al. (1982, 1988)
D_v	$6.9 \times 10^{-4} \exp(-5.35 \times 10^{-19}/kT)$ ($m^2\ s^{-1}$)	Kogai (1997) and Reynolds and Burton (1979)
$F_{c,sat}$	0.5	e.g., Veshchunov (2008) and White (2004)
k	$1.38 \times 10^{-23}\ J\ K^{-1}$	–
l_f	6×10^{-6} m	White and Tucker (1983)
$N_{gf,0}$	$4 \times 10^{13}\ m^{-2}$	Cheon et al. (2004) and White (2004)
N_{ig}	$7 \times 10^{23}\ m^{-3}$	Olander and Wongsawaeng (2006)
Z_0	10^{-9} m	White and Tucker (1983)
γ	$1\ J\ m^{-2}$	Kogai (1997)
δ_g	5×10^{-10} m	Kogai (1997)
θ	50°	e.g., Koo et al. (2000) and White (2004)
ω	$8.5 \times 10^{-29}\ m^3$	–
Ω_{gf}	$4.09 \times 10^{-29}\ m^3$	Kogai (1997)
Ω_{ig}	$3 \times 10^{-29}\ m^3$	Olander and Wongsawaeng (2006)

Table 2
Details of irradiation tests and SEM analyses of the AGR/Halden Ramp Test Programme (White et al., 2006).

Rod identifier	Burn-up (GWd/t)	Ramp type	Peak power ($kW\ m^{-1}$)	Holding time	SEM zones	Boundaries measured
4000	20.7	Fast	40	30.0 min	5	48
4004	20.5	Fast	40	2.38 min	6	44
4005	20.8	Fast	40	2.0 min	5	39
4064	20.1	Slow	43	–	5	63
4065	9.3	Slow	41.8	–	5	43
4159	20.2	Cycled	18–26	115 × 4 h	5	56
4160	20.1	Cycled	18–26	115 × 4 h	6	45
4162	12.6	Slow	40	–	4	47
4163	12.6	Fast	40	2.0 min	5	37
					46	422

Table 3
Details of power ramps in the irradiation tests of the AGR/Halden Ramp Test Programme (White et al., 2006).

Rod identifier	Power 1 ($kW\ m^{-1}$)	τ_1	τ_{2a} (min)	Power 2 ($kW\ m^{-1}$)	τ_{2b} (min)	τ_{2c} (s)	Power 3 ($kW\ m^{-1}$)	τ_3 (min)	τ_4
4000	14.0	12d	1.52	40.0	30.0	100	14.0	99.0	SCRAM
4004	14.0	12d	1.97	40.0	2.38	90	14.0	99.0	SCRAM
4005	14.0	12d	1.32	40.0	2.0	–	SCRAM	–	–
4064	20.0	15wk	47.0	43.0	0.0	–	SCRAM	–	–
4065	19.3	3wk	47.0	41.8	0.0	–	SCRAM	–	–
4162	18.0	3wk	45.0	40	0.0	40	18.0	6	–
4163	18.0	3wk	2.0	40.0	2.0	80	SCRAM	–	–

The two power-cycled fuel rods were subjected to 115 four-hour cycles, the details of which are summarised in Table 4.

For each test, the SEM examinations were performed at different zones of the fuel specimen, allowing the construction of a wide database of grain-face swelling measurements. Moreover, the specific power, temperature, and hydrostatic stress for each SEM zone were evaluated by means of the ENIGMA code (Rossiter, 2011), thus providing the basis for reconstruction of the experiments and verification of fission gas behaviour models. In Table 5, a summary of the experimental data of fractional volume grain-face swelling for each SEM zone is given.

3.2. Calculations

The simulations of the ramp tests from the AGR/Halden Ramp Test Programme were carried out coherently with the fuel fabrication data and the details of the irradiation histories provided in (White et al., 2006). Moreover, the following assumptions were made in order to assess the initial conditions for the analysis of the ramp tests:

- All the fission gas generated during the base-irradiation is considered to be retained inside the fuel grains at the beginning of

Table 4
Details of power cycles in the irradiation tests of the AGR/Halden Ramp Test Programme (White et al., 2006).

Rod identifier	Power 1 ($kW\ m^{-1}$)	Time 1	Ramp up	Power up ($kW\ m^{-1}$)	Ramp down	Power down ($kW\ m^{-1}$)	De-conditioning ($kW\ m^{-1}$)	Last phase
4159 and 4160	18.0	7d	30 min	26.0 for 1 h	30 min 115–4 h cycles	18.0 for 2 h	18.0 for 2d	Shut-down

Table 5
Summary of experimental data of grain-face swelling considered in the present work (White et al., 2006).

SEM zone	$(\Delta V/V)_{gf}$ (%)	SEM zone	$(\Delta V/V)_{gf}$ (%)	SEM zone	$(\Delta V/V)_{gf}$ (%)
4000-A	0.97 ± 0.35	4064-A	1.07 ± 0.58	4160-A	2.61 ± 0.57
4000-B	0.68 ± 0.12	4064-B	0.86 ± 0.32	4160-B	2.30 ± 0.56
4000-C	0.53 ± 0.10	4064-C	0.63 ± 0.22	4160-C	2.60 ± 0.36
4000-D	0.46 ± 0.10	4064-D	0.74 ± 0.19	4160-D	1.64 ± 0.20
4000-F	0.17 ± 0.4	4064-E	0.59 ± 0.26	4160-E	1.22 ± 0.21
				4160-F	0.74 ± 0.09
4004-A	0.62 ± 0.13	4065-A	1.25 ± 0.43	4162-A	0.70 ± 0.26
4004-B	0.70 ± 0.26	4065-B	1.35 ± 0.30	4162-B	0.46 ± 0.17
4004-C	0.44 ± 0.11	4065-C	0.97 ± 0.26	4162-C	0.43 ± 0.18
4004-D	0.56 ± 0.15	4065-D	0.79 ± 0.15	4162-D	0.43 ± 0.22
4004-E	0.27 ± 0.07	4065-E	0.21		
4004-F	0.16				
4005-A	0.94 ± 0.16	4159-A	1.85 ± 0.22	4163-A	0.60 ± 0.20
4005-B	0.57 ± 0.20	4159-B	1.67 ± 0.26	4163-B	0.59 ± 0.18
4005-C	0.42 ± 0.12	4159-C	1.37 ± 0.16	4163-C	0.35 ± 0.10
4005-D	0.54 ± 0.15	4159-D	1.06 ± 0.15	4163-D	0.40 ± 0.06
4005-E	0.27 ± 0.02	4159-E	0.91 ± 0.28	4163-E	0.26 ± 0.13

the calculation. This hypothesis is consistent with the observation that, in all of the studied cases, the base-irradiation resulted in negligible fission gas release and micro-structural changes (White et al., 2006).

- The fuel grain size is assumed to remain constant at the final (measured) value throughout the ramp test. Grain growth calculations based on the model of the TRANSURANUS code (Ainscough et al., 1973; Lassmann et al., 2011) showed that the predicted grain growth is lower than or comparable to the experimental scatter for the grain size data (White et al., 2006) in all the analysed cases.

An example of calculation is presented in Fig. 3. During the conditioning time, τ_1, the bubble over-pressure is very high ($p/p_{eq} \approx 30$–40 in this case). The subsequent increase in temperature following the power ramp leads to rapid growth of grain-face bubbles caused by an increase of the intra-granular gas diffusion and of the vacancy absorption rate (Section 2). Consequently, the grain-face swelling increases and FGR commences. It can be noted that the model predicts the incubation behaviour of the FGR. Also, the coupling between FGR and swelling is consistently described, since the swelling rate is reduced by loss of gas from the grain faces as FGR takes place.

The comparison of the calculations with all the experimental data of grain-face swelling considered in the present work (Table 5) is shown in Fig. 4. The results point out a reasonable overall agreement, without any fitting applied to the model parameters. Although an average under-estimation of the experimental values is observed, the level of accuracy appears to be consistent with the uncertainties pertaining to the parameters and satisfactory in view of the application of the new model to integral fuel rod analysis.

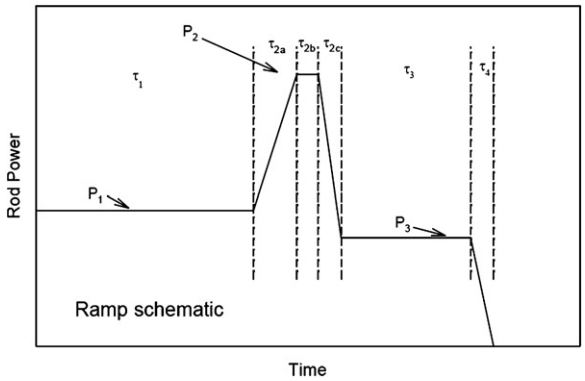

Fig. 2. Schematic of a generic power ramp test of the AGR/Halden Ramp Test Programme (White et al., 2006). The parameters for each case are reported in Table 3.

4. Model testing in the TRANSURANUS code

The applicability of the new model to integral fuel rod analysis was verified through implementation and testing in the

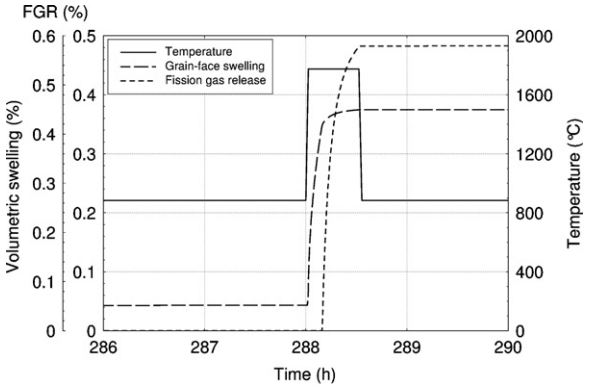

Fig. 3. Grain-face swelling and fission gas release (defined as the ratio of the released to the generated gas) for the SEM zone 4000-A, calculated using the new model. The temperature (White et al., 2006) is also shown. The figure zooms in on the ramp.

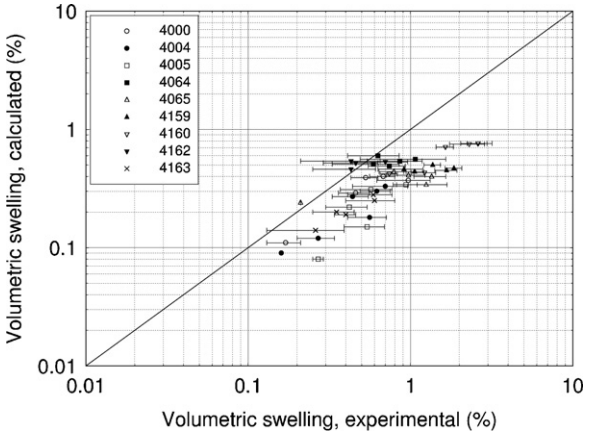

Fig. 4. Comparison between values of grain-face swelling calculated using the new model and the experimental data from (White et al., 2006).

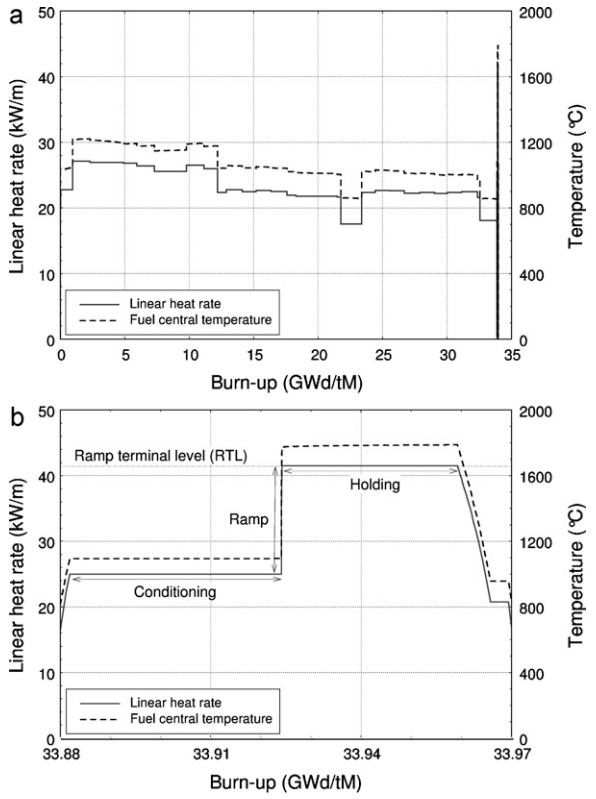

Fig. 5. Linear heat rate and fuel central temperature as a function of the burn-up at the mid-plane of the PK1-1 fuel rod. (a) Entire irradiation time and (b) zoom on the ramp test.

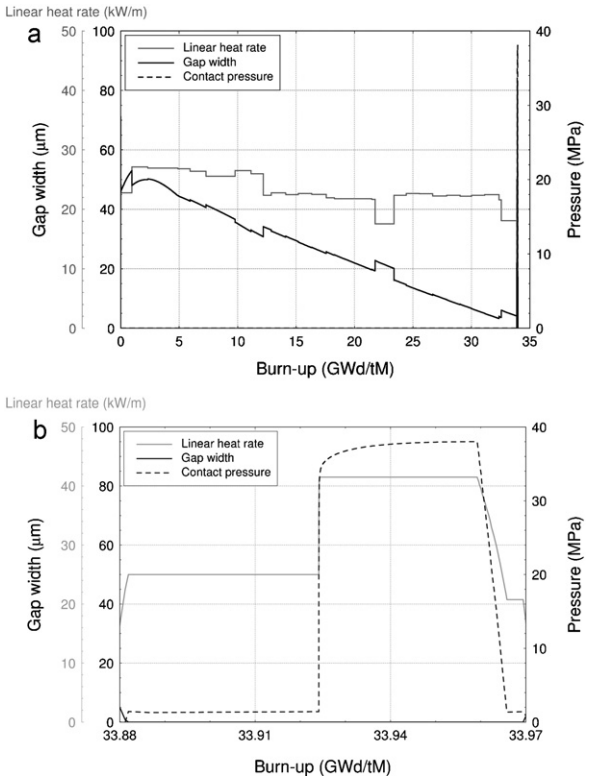

Fig. 6. Linear heat rate, radial gap width and fuel-cladding contact pressure as a function of the burn-up at the mid-plane of the PK1-1 fuel rod. (a) Entire irradiation time and (b) zoom on the ramp test.

TRANSURANUS fuel rod analysis code. The model was coupled with the TRANSURANUS subprograms for the calculation of the fission gas generation rate and the solution of the intra-granular gas diffusion equation. Also, the TRANSURANUS models were adopted for taking into account the athermal release mechanisms (recoil and knock-out) and the grain boundary sweeping effect (Van Uffelen et al., 2010). The flexibility of the code allowed obtaining an effective implementation, without modifying the solution methods of the thermal–mechanical analysis. Through a consistent matching between the new model and the pre-existing structure of TRANSURANUS, the multiple feedback effects between the fission gas swelling and release calculations and the thermal–mechanical analysis are taken into account in the calculations, among which the dependence of these phenomena on the local hydrostatic stress in the fuel. Adopting the new model, the TRANSURANUS code was employed for the analysis of fuel rod irradiation experiments from the IFPE database, as discussed in Sections 4.1, 4.2 and 4.3.

4.1. Experimental databases

The databases of the Super-Ramp (PWR subprogram) and Inter-Ramp Projects (Djurle, 1979, 1984) refer to PWR-UO_2 and BWR-UO_2 fuel rods, respectively, power ramp-tested in the Studsvik reactor R2 after base-irradiation up to moderate burn-up. The Super-Ramp rods were base-irradiated in a burn-up range of 28–45 GWd/t, while the Inter-Ramp rods experienced burn-up of 8–20 GWd/t. Several fuel rods with different design parameters (i.e., gap width, fuel density and grain size, ^{235}U enrichment, annular and solid pellets, gadolinium content) were tested. The main pre-irradiation characterization data for the different groups of rods are summarised in Tables 6 and 7. A typical base-irradiation and power ramp irradiation history is shown in Fig. 5, and the power ramp test features for all the fuel rods considered in the present work are reported in Tables 8 and 9. The ramp test consists of a conditioning time and a subsequent power ramp, followed by a holding time at the ramp terminal level (RTL), and reactor shut-down. With reference to an extensive experimental analysis program and to detailed records of fuel rod power histories, wide experimental databases were constructed during the Super-Ramp and Inter-Ramp Projects, which were made available through the IFPE database and were considered within the FUMEX-III Project of the IAEA.

4.2. Integral fuel rod analyses

The fuel rod irradiation experiments from the Super-Ramp and Inter-Ramp Projects were simulated in the present work by means of the TRANSURANUS code, using the new implemented model of fission gas swelling and release. In this sub-section, the exemplifying case of the PK1-1 fuel rod from the Super-Ramp Project is discussed, which is representative of the general model capabilities observed for the whole set of simulations. Fig. 5 shows the linear heat rate and the calculated fuel central temperature at the axial power peak position (fuel rod mid-plane) as a function of the burn-up. Fig. 6 displays the radial width of the fuel-cladding gap, and the fuel-cladding contact pressure at the fuel rod mid-plane as a function of the burn-up. At the beginning of the conditioning time, the gap closes and pellet-cladding mechanical interaction (PCMI) occurs, leading to the onset of contact pressure. The contact pressure strongly increases during the power ramp as a consequence of the fuel swelling and the differential thermal expansion of the fuel and the cladding.

The calculated volumetric fission gas swelling, FGR and temperature at the mid-plane of the PK1-1 fuel rod for different values of burn-up are displayed in Fig. 7, as a function of the pellet radius. The summation of the intra-granular and grain-face swelling is

Table 6
Pre-irradiation data and average burn-up for the different groups of PWR fuel rods from the Super-Ramp Project (Djurle, 1984).

Group	Pellet type	Average burn-up at EOL (GWd/t)	Diametral gap width (μm)	UO_2 density (%TD)	Average grain size (μm)	Enrichment (wt% ^{235}U)
PK1	Standard	33–36	191–200	95	6.0	3.20
PK2	Standard	41–45	145	94	5.5	3.21
PK4	Gd_2O_3 (4.1 wt%)	33–34	167–169	94	5.5	3.19
PK6	Large grain	34–37	145–146	95	22.0	2.99
PW3	Standard	28–31	170	94	10.5	8.26
PW5	Annular	32–33	162–165	95	16.9	5.74

Table 7
Pre-irradiation data and average burn-up for the different groups of BWR fuel rods from the Inter-Ramp Project (Djurle, 1979).

Group	Pellet type	Average burn-up at EOL (GWd/t)	Diametral gap width (μm)	UO_2 density (%TD)	Average grain size (μm)	Enrichment (wt% ^{235}U)
LR	Standard	8.5–10.3	150	95	8.3	2.82
LS	Standard	8.2–10.4	150	95	8.3	2.82
TR	Standard	10	80	95	8.3	2.82
TS	Standard	9.8	80	95	8.3	2.82
DR	Standard	7.9	150	93	10.9	2.82
HR	Standard	16.6–19.8	150	95	8.4	3.50
HS	Standard	16.6–19.3	150	95	8.4	3.50
BR	Standard	19.9	250	95	8.4	3.50

Table 8
Features of the ramp tests in axial power peak position for the Super-Ramp PWR fuel rods considered in the present work (Djurle, 1984).

Rod	Conditioning power level (kW m^{-1})	Conditioning time (min)	Power ramp rate (kW m^{-1} min^{-1})	Ramp terminal level (kW m^{-1})	Holding time at RTL (min)
PK1-1	25.0	1440	9.0	41.5	720
PK1-2	25.0	1440	8.0	44.0	720
PK1-3	25.0	1440	8.5	47.5	720
PK1-4	25.0	1440	9.5	47.5	720
PK2-1	25.0	1440	8.5	41.0	720
PK2-2	25.0	1440	9.5	46.0	720
PK2-3	25.0	1440	8.5	49.0	720
PK2-4	25.0	1440	8.5	44.0	1
PK2-S	25.0	1440	8.5	44.0	720
PK4-1	25.0	1440	8.0	39.0	720
PK4-2	25.0	1440	8.5	44.5	720
PK4-3	25.5	1440	11.0	50.5	720
PK6-2	25.5	1440	9.0	40.0	720
PK6-3	25.0	1440	9.0	43.0	720
PK6-S	24.0	1440	10.0	41.0	720
PW3-2	25.5	1440	10.0	35.3	720
PW3-3	25.0	1440	10.0	37.2	720

considered. The grain-face swelling, however, was found to be the dominant contribution to the calculated fission gas swelling in all the analysed cases. As shown in Fig. 7, both the swelling and the FGR decrease with increasing distance from the pellet centre, reflecting the spatial dependence of the temperature in the fuel. In fact, the temperature drives both the inflow of gas atoms and the absorption of vacancies at the grain-face bubbles, thus determining the bubble growth and coalescence rate, and in turn the fission gas swelling and release (Section 2). As predicted by the model, thermal FGR does not occur beyond a certain distance from the pellet centre. The fuel zone, which is not affected by significant FGR, lies towards the decreasing temperatures, where the condition of grain face saturation is not attained. It is also noticed that the swelling gradient abruptly changes at the radial position delimiting the zone where FGR takes place. In fact, FGR results in reduction of the amount of gas retained at the grain faces and consequently interacts with the

Table 9
Features of the ramp tests in axial power peak position for the Inter-Ramp BWR fuel rods considered in the present work (Djurle, 1979).

Rod	Conditioning power level (kW m^{-1})	Conditioning time (min)	Power ramp rate (kW m^{-1} min^{-1})	Ramp terminal level (kW m^{-1})	Holding time at RTL (min)
LR1	29.8	1440	4.8	43.8	1440
LS2	31.8	1440	3.9	43.8	1440
LS3	25.0	1440	3.9	41.8	1440
TR1	30.7	1440	4.2	42.2	1440
DR1	22.9	1440	4.5	43.2	1440
HR2	23.0	1440	4.5	38.0	1440
HR4	29.0	1440	4.2	46.1	1440
HR5	29.0	1440	4.2	47.9	1440
HS1	30.3	1440	3.9	47.8	26
HS2	24.8	1440	3.9	41.0	1440
BR1	31.1	1440	3.9	51.0	1440

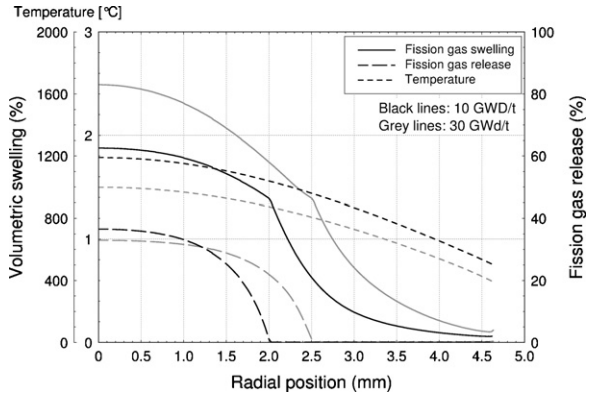

Fig. 7. Fission gas swelling, fission gas release and temperature as a function of the pellet radius at the mid-plane of the PK1-1 fuel rod. The figure refers to two different burn-up values of 10 GWd/t and 30 GWd/t.

grain-face swelling. The curves presented in Fig. 7 therefore reflect the physical basis of the model and reveal a consistent coupling between the fission gas swelling and release (formerly not considered in the TRANSURANUS code), as well as their dependence on the temperature. The comparison between the results at 10 and 30 GWd/t in Fig. 7 points out that the model captures the dependence of both phenomena on the burn-up. In particular, the swelling tends to increase with burn-up due to the progressive inflow of gas atoms and absorption of vacancies at the grain-face bubbles. Grain-face bubble growth with burn-up is also reflected in progressive broadening of the fuel portion affected by thermal FGR. The effect of burn-up was observed experimentally by a shift of a dark ring in electron probe micro-analysis (Sontheimer and Landskron, 1999).

The radial profiles of fission gas swelling, hydrostatic stress and temperature for the PK1-1 rod at the beginning of the holding time (see Fig. 5) are shown in Fig. 8. Following the power ramp, high compressive hydrostatic stress takes place in the central zone of the fuel pellet, which is due to strong PCMI and the consequent fuel-cladding contact pressure (Fig. 6), as well as due to increased thermal stress. The grey line in Fig. 8 represents the swelling profile calculated by neglecting the hydrostatic stress in the model calculations. The effect of the compressive stress in constraining the swelling, as reproduced by the new model, is noticeable.

The calculated integral fission gas release and fuel central temperature as a function of the burn-up for the PK1-1 fuel rod are presented in Fig. 9. The incubation behaviour and temperature-dependence of the FGR is well reproduced. Fig. 10 compares the integral FGR during the ramp test as a function of the burn-up with that obtained by neglecting the hydrostatic stress. The radially averaged hydrostatic stress in the fuel as a function of the burn-up is also displayed. It is worth emphasizing that the new model consistently takes into account the local hydrostatic stress. The radially averaged value is presented in Fig. 10 only as indicative of the development of a high compressive hydrostatic stress during the power ramp test. As for the complementary phenomenon of fission gas swelling, the FGR is remarkably affected by the hydrostatic stress during the power ramp test.

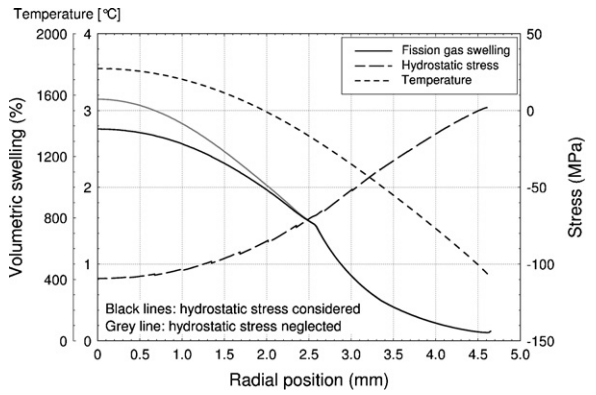

Fig. 8. Fission gas swelling, hydrostatic stress (considered to be negative if compressive) and temperature as a function of the pellet radius at the mid-plane of the PK1-1 fuel rod. The fission gas swelling obtained by neglecting the hydrostatic stress is also shown. The figure refers to the beginning of the holding time.

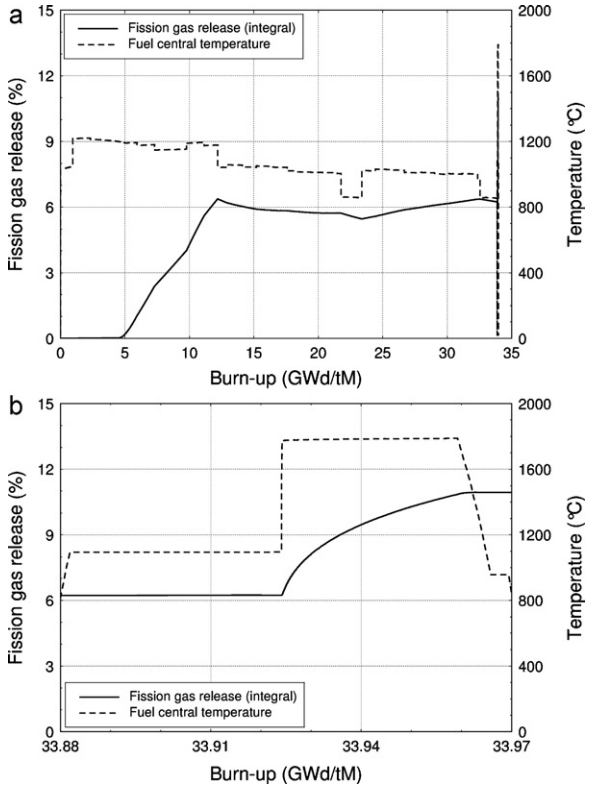

Fig. 9. Integral fission gas release and fuel central temperature as a function of the burn-up at the mid-plane of the PK1-1 fuel rod. (a) Entire irradiation time and (b) zoom on the ramp test.

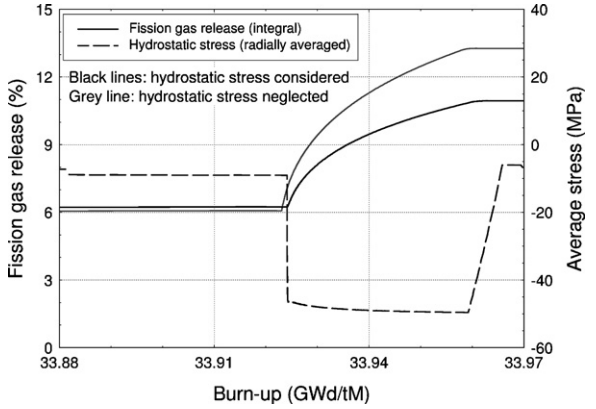

Fig. 10. Integral fission gas release and radially averaged hydrostatic stress in the fuel as a function of the burn-up at the mid-plane of the PK1-1 fuel rod. Both FGR curves obtained by considering and by neglecting the hydrostatic stress are shown. The figure zooms in on the ramp test.

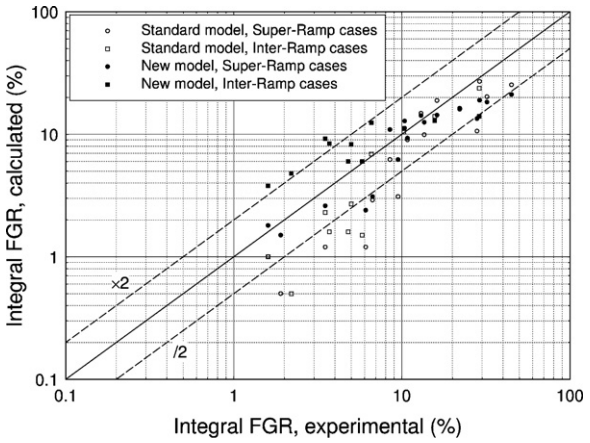

Fig. 11. Comparison between the calculated values of integral fission gas release at the EOL and the experimental data for the Super-Ramp and the Inter-Ramp cases. Both the results obtained by adopting the standard model of the TRANSURANUS code and the new model are shown.

4.3. Comparison with experimental data of integral FGR

As a preliminary validation of the new model implemented in the TRANSURANUS code, the results of the performed fuel rod analyses were systematically compared with the experimental values of integral FGR. Given the interrelation between the integral FGR and the other multiple aspects of the fuel rod thermal–mechanical behaviour, the results presented in this sub-section may be considered as indicative of the overall performance of the new model implemented in the TRANSURANUS code.

Experimental data of integral FGR at the end of life (EOL) are available for 17 rods of the Super-Ramp Project and 11 rods of the Inter-Ramp Project. All these cases (Tables 8 and 9) are considered here. The comparison between the TRANSURANUS predictions and the experimental values is presented in Fig. 11. Both the results obtained by adopting the standard model of the TRANSURANUS code (Lassmann et al., 2011) and the new model are shown. When the standard model is used, a systematic under-estimation of the experimental data is observed, and the predicted values deviate on average from the experimental ones by a factor of about 2.1. By using the new model, the obtained average deviation from the experimental values is of a factor of about 1.6, and the systematic under-estimation appears to be overcome, leading to an improvement of the TRANSURANUS predictions. However, a significant over-estimation is observed of the FGR values lower than 10%. Indeed, it is known that the region of FGR of the order of 1% is extremely difficult to be predicted accurately (IAEA, 1998). It is concluded that the new model of fission gas swelling and release implemented in the TRANSURANUS code allows obtaining a reasonable predictive accuracy in terms of integral FGR.

5. Summary and conclusions

In this paper, a physics-based model was developed for analysing the coupled phenomena of fission gas swelling and release in UO_2 fuel during irradiation. The model incorporates the fundamental physical processes of gas diffusion and precipitation in grains, growth and coalescence of the grain-face gas bubbles, and gas release to the fuel rod free volume. Mathematical approaches from the literature were revisited and combined in a practical treatment, comprising an improvement of the model of White for grain-face bubble coalescence.

The new model was firstly coded as stand-alone version and preliminarily assessed through the analysis of irradiation experiments from the IFPE database, pointing out a reasonable agreement between the predictions and the available experimental data of grain-face swelling.

The applicability of the new model to integral fuel rod analysis was verified through implementation and testing in the TRANSURANUS code. Consistent matching was provided between the stress-dependent fission gas swelling and release calculations and the whole thermal–mechanical analysis. From the simulation of irradiation experiments of LWR fuel rods from the IFPE database, some of which were also considered within the FUMEX-III Project of the IAEA, the following main conclusions can be drawn:

- The new model, implemented in the TRANSURANUS code, reproduces the main peculiarities of the fission gas swelling and release, in accordance with the observations reported in the literature. In particular, the intrinsic coupling between the fission gas swelling and release, the dependence of both phenomena on the local hydrostatic stress, and the incubation behaviour of the FGR are consistently described.
- Combined with the characteristics of the TRANSURANUS code, the new model allows obtaining a reasonable predictive accuracy in terms of integral FGR, along with some improvements compared to the standard TRANSURANUS model, without any fitting applied to the model parameters.
- The implementation of the new model represents a step forward in the development of the TRANSURANUS code. The improvements are mainly related to the advantages and the flexibility of a physics-based treatment, compared to the previously adopted empirical and semi-empirical approaches. Moreover, taking into account the dependence of the fission gas swelling and release on the local hydrostatic stress is of high importance for the improved analysis of the fuel rod behaviour under PCMI conditions, which is topical in view the tendency to extend the discharge burn-up and the flexibility of use of the nuclear fuel.

Finally, the new model provides a basis for integrating further physical details. In particular, advisable developments include:

- Introducing a more suitable treatment of the intra-granular gas behaviour. This refinement will require taking into account the mobility and variable number density of the intra-granular gas bubbles (e.g., according to Van Uffelen et al., 2011), as well as intra-granular bubble coalescence.
- Considering the high-burn-up-induced mechanisms of fission gas swelling and release.
- Introducing a physics-based treatment of the athermal gas release mechanisms.
- Developing a model for grain-face bubble nucleation.
- Taking into account the burst release effect due to micro-cracking of the fuel pellets and consequent grain boundary opening during fast power changes.

Acknowledgements

This work was partly supported by the Ph.D. grant for G. Pastore from Politecnico di Milano, and the support for mobility of the researchers from ITU. The authors also acknowledge E. Sartori from the OECD/NEA and J. Killeen from the IAEA for maintaining and developing the IFPE Database. A special thank is due to Klaus Lassmann for the valuable advice and scientific support.

References

Ainscough, J.B., Oldfield, B.W., Ware, J.O., 1973. Isothermal grain growth kinetics in sintered UO_2 pellets. J. Nucl. Mater. 49, 117–128.
Aybar, H.S., Ortego, P., 2005. A review of nuclear fuel performance codes. Prog. Nucl. Energy 46 (2), 127–141.

Bernard, L.C., Bonnaud, E., 1997. Finite volume method for fission gas release modeling. J. Nucl. Mater. 244, 75–84.
Bernard, L.C., Jacoud, J.L., Vesco, P., 2002. An efficient model for the analysis of fission gas release. J. Nucl. Mater. 302, 125–134.
Calvin, C., Nowak, D., 2010. High performance computing in nuclear engineering. In: Cacuci, D.G. (Ed.), Handbook of Nuclear Engineering, vol. 12. Springer Science + Business Media, LLC., New York, NY, USA, pp. 1449–1517.
Cheon, J.-S., Koo, Y.-H., Lee, B.-H., Oh, J.-Y., Sohn, D.-S., 2004. Modeling of a pellet-clad mechanical interaction in LWR fuel by considering gaseous swelling. In: Proc. Int. Seminar on Pellet-Clad Interaction in Water Reactor Fuels, Aix-en-Provence, France, pp. 191–201.
Djurle, S., 1979. The Studsvik Inter-Ramp Project. Final Report STUDSVIK-STIR-53.
Djurle, S., 1984. The Super-Ramp Project. Final Report STUDSVIK-STSR-32.
Garcia, P., Martin, G., Sabathier, C., Carlot, G., Michel, A., Martin, P., Dorado, B., Freyss, M., Bertolus, M., Skorek, R., Noirot, J., Noirot, L., Kaitasov, O., Maillard, S., 2012. Nucleation and growth of intragranular defect and insoluble atom clusters in nuclear oxide fuels. Nucl. Instrum. Methods Phys. Res. B 277, 98–108.
Geelhood, K., 2011. Recent updates to NRC fuel performance codes and plans for future improvements. Nucl. Eng. Technol. 43 (6), 509–522.
Govers, K., Lemehov, S., Verwerft, M., 2008. In-pile Xe diffusion coefficient in UO_2 determined from the modeling of intragranular bubble growth and destruction under irradiation. J. Nucl. Mater. 374, 461–472.
Griger, Á., Gadó, J., 2007. Models of the FUROM-1.3 Code. AEKI-FRL-2007-719-1. 3-01 (in Hungarian).
Ham, F.S., 1958. Theory of diffusion-limited precipitation. J. Phys. Chem. Solids 6, 335–351.
Harriague, S., Coroli, G., Savino, E.J., 1980. BACO (Barra Combustible), a computer code for simulating a reactor fuel rod performance. Nucl. Eng. Des. 56, 91–103.
IAEA, 1998. Fuel Modelling at Extended Burnup. Technical Report IAEA-TECDOC-998.
Kashibe, S., Une, K., 1997. Effect of external restraint on bubble swelling in UO_2 fuels. J. Nucl. Mater. 247, 138–146.
Kashibe, S., Une, K., Nogita, K., 1993. Formation and growth of intragranular fission gas bubbles in UO_2 fuels with burnup of 6–83 GWd/t. J. Nucl. Mater. 206, 22–34.
Khvostov, G., Mikityuk, K., Zimmermann, M.A., 2011. A model for fission gas release and gaseous swelling of the uranium dioxide fuel coupled with the FALCON code. Nucl. Eng. Des. 241, 2983–3007.
Killeen, J., Sartori, E., McGrath, M., 2009. FUMEX-III: a new IAEA coordinated research project on fuel modelling at extended burnup. In: Proc. Int. Conf. on Water Reactor Fuel Performance, Paris, France, pp. 336–343.
Kogai, T., 1997. Modelling of fission gas release and gaseous swelling of light water reactor fuels. J. Nucl. Mater. 244, 131–140.
Kogai, T., Ito, K., Iwano, Y., 1988. The effect of cladding restraint on fission gas release behavior. J. Nucl. Mater. 158, 64–70.
Koo, Y.-H., Lee, B.-H., Sohn, D.-S., 2000. Analysis of fission gas release and gaseous swelling in UO_2 fuel under the effect of external restraint. J. Nucl. Mater. 280, 86–98.
Lassmann, K., 1980. The structure of fuel element codes. Nucl. Eng. Des. 57, 17–39.
Lassmann, K., 1992. TRANSURANUS: a fuel rod analysis code ready for use. J. Nucl. Mater. 188, 295–302.
Lassmann, K., Schubert, A., Van Uffelen, P., Győri, C., van de Laar, J., 2011. TRANSURANUS Handbook. Copyright ©1975–2011. Institute for Transuranium Elements, Karlsruhe, Germany.
Lee, B.-H., Koo, Y.-H., Oh, J.-Y., Cheon, J.-S., Tahk, Y.-W., Sohn, D.-S., 2011. Fuel performance code COSMOS for analysis of LWR UO_2 and MOX fuel. Nucl. Eng. Technol. 43 (6), 499–508.
Lösönen, P., 2002. Modelling intragranular fission gas release in irradiation of sintered LWR UO_2 fuel. J. Nucl. Mater. 304, 29–49.
Massih, A.R., Forsberg, K., 2008. Calculation of grain boundary gaseous swelling in UO_2. J. Nucl. Mater. 377, 406–408.
Matzke, H., 1980. Gas release mechanisms in UO_2 – a critical review. Radiat. Eff. 53, 219–242.
Mikityuk, K., Shestopalov, A., 2011. FRED fuel behaviour code: main models and analysis of Halden IFA-503.2 tests. Nucl. Eng. Des. 241, 2455–2461.
Mogensen, M., Bagger, C., Walker, C.T., 1993. An experimental study of the distribution of retained xenon in transient-tested UO_2 fuel. J. Nucl. Mater. 199, 85–101.
Nakamura, J., Suzuki, M., Uetsuka, H., 1999. Re-irradiation tests of LWR spent fuel at JMTR. In: EHPG Meeting, Loen, Norway.
OECD/NEA, 2004. Pellet-clad interaction in water reactor fuels. In: Seminar Proceedings, Aix-en-Provence, France.
Olander, D.R., 1976. Fundamental Aspects of Nuclear Reactor Fuel Elements. Technical Information Center – Energy Research and Development Administration, University of California, Berkeley.
Olander, D.R., Van Uffelen, P., 2001. On the role of grain boundary diffusion in fission gas release. J. Nucl. Mater. 288, 137–147.
Olander, D.R., Wongsawaeng, D., 2006. Re-solution of fission gas – a review: Part I. Intragranular bubbles. J. Nucl. Mater. 354, 94–109.
Rest, J., 2003. The effect of irradiation-induced gas-atom re-solution on grain-boundary bubble growth. J. Nucl. Mater. 321, 305–312.
Reynolds, G.L., Burton, B., 1979. Grain-boundary diffusion in uranium dioxide: the correlation between sintering and creep and a reinterpretation of creep mechanism. J. Nucl. Mater. 82, 22–25.
Rossiter, G., 2011. Development of the ENIGMA fuel performance code for whole core analysis and dry storage assessments. Nucl. Eng. Technol. 43 (6), 489–498.
Sartori, E., Killeen, J., Turnbull, J.A., 2010. International Fuel Performance Experiments (IFPE) Database, OECD-NEA. Available at http://www.oecd-nea.org/science/fuel/ifpelst.html
Schubert, A., Botazzoli, P., Boneva, S., Di Marcello, V., Pastore, G., van de Laar, J., Van Uffelen, P., 2011. Application of the extended TRANSURANUS code in the FUMEX-III project. In: Proc. of the 9th Int. Conf. on WWER Fuel Performance, Modelling and Experimental Support, Bourgas, Bulgaria.
Sontheimer, F., Landskron, H., 1999. Puzzling features of EPMA radial fission gas release profiles: the key to realistic modelling of fission gas release up to ultra high burnup. In: Proc. of Enlarged Halden Programme Group Meeting, vol. 1, OECD Halden Reactor Project, Loen, Norway.
Speight, M.V., 1969. A calculation on the migration of fission gas in material exhibiting precipitation and re-solution of gas atoms under irradiation. Nucl. Sci. Eng. 37, 180–185.
Speight, M.V., Beere, W., 1975. Vacancy potential and void growth on grain boundaries. Met. Sci. 9, 190–191.
Suzuki, M., Saitou, H., 2006. Light Water Reactor Fuel Analysis Code FEMAXI-6 (Ver. 1). JAEA-Data/Code 2005-003, Japan Atomic Energy Agency.
Turnbull, J.A., 1971. The distribution of intragranular fission gas bubbles in UO_2 during irradiation. J. Nucl. Mater. 38, 203–212.
Turnbull, J.A., Friskney, C.A., Findlay, J.R., Johnson, F.A., Walter, A.J., 1982. The diffusion coefficients of gaseous and volatile species during the irradiation of uranium dioxide. J. Nucl. Mater. 107, 168–184.
Turnbull, J.A., White, R.J., Wise, C.A., 1988. The diffusion coefficient for fission gas atoms in uranium dioxide. In: Proc. of Technical Committee Meeting on Water Reactor Fuel Element Computer Modelling in Steady State, Transient and Accidental Conditions, Preston, England.
Van Uffelen, P., Konings, R.J.M., Vitanza, C., Tulenko, J., 2010. Analysis of reactor fuel rod behavior. In: Cacuci, D.G. (Ed.), Handbook of Nuclear Engineering, vol. 13. Springer Science + Business Media, LLC., New York, NY, USA, pp. 1519–1627.
Van Uffelen, P., Pastore, G., Di Marcello, V., Luzzi, L., 2011. Multiscale modelling for the fission gas behaviour in the TRANSURANUS code. Nucl. Eng. Technol. 43 (6), 477–488.
Van Uffelen, P., Sheindlin, M., Rondinella, V., Ronchi, C., 2004. On the relations between the fission gas behaviour and the pellet-cladding mechanical interaction in LWR fuel rods. In: Proc. of the Int. Seminar on Pellet-Clad Interaction in Water Reactor Fuels, Aix-en-Provence, France, pp. 213–228.
Veshchunov, M.S., 2008. Modelling of grain face bubbles coalescence in irradiated UO_2 fuel. J. Nucl. Mater. 374, 44–53.
White, R.J., 1994. A new mechanistic model for the calculation of fission gas release. In: Proc. of the Int. Topical Meeting on Light Water Reactor Fuel Performance, West Palm Beach, FL, USA, pp. 196–202.
White, R.J., 2004. The development of grain-face porosity in irradiated oxide fuel. J. Nucl. Mater. 325, 61–77.
White, R.J., Corcoran, R.C., Barnes, J.P., 2006. A Summary of Swelling Data Obtained from the AGR/Halden Ramp Test Programme. Report R&T/NG/EXT/REP/0206/02.
White, R.J., Tucker, M.O., 1983. A new fission-gas release model. J. Nucl. Mater. 118, 1–38.
Zimmermann, H., 1978. Investigations on swelling and fission gas behaviour in uranium dioxide. J. Nucl. Mater. 75, 154–161.